Acta Cryst C STRUCTURAL CHEMISTRY

ISSN 2053-2296

The disordered structure of sparsentan: energy calculations for competing chain conformations

Thomas Gelbrich,[a,b]* Kristaps Saršūns[a,b] and Doris E. Braun[a,b]*

[a]Christian Doppler Laboratory for Advanced Crystal Engineering Strategies in Drug Development, Innrain 52c, Innsbruck, 6020, Austria, and [b]Institute of Pharmacy, University of Innsbruck, Innrain 52c, Innsbruck, 6020, Austria. *Correspondence e-mail: thomas.gelbrich@uibk.ac.at, doris.braun@uibk.ac.at

Received 17 June 2025
Accepted 12 August 2025

Edited by X. Wang, Oak Ridge National Laboratory, USA

Keywords: crystal structure; disorder; energy calculations; conformation; pharmaceutical; flexible molecule; sparsentan; SST.

CCDC reference: 2480328

Supporting information: this article has supporting information at journals.iucr.org/c

The crystalline form of sparsentan (SST) (systematic name: 2-{4-[(2-butyl-4-oxo-1,3-diazaspiro[4.4]non-1-en-3-yl)methyl]-2-(ethoxymethyl)phenyl}-*N*-(4,5-dimethyl-1,2-oxazol-3-yl)benzenesulfonamide), $C_{32}H_{40}N_4O_5S$, was produced and characterized using single-crystal and powder X-ray diffraction, differential scanning calorimetry (DSC), thermogravimetric analysis (TGA) and IR spectroscopy. The SST molecule displays positional disorder in three different sections. Viability tests of alternative disorder models involved the calculation of energetic contributions to analyse each possible molecular conformation within its crystal environment and identify the energetically most favourable conformations in the lattice.

1. Introduction

Sparsentan (SST, Scheme 1) is a dual endothelin type A (ETA) receptor and angiotensin II type 1 (AT1) receptor antagonist (DEARA), developed by Travere Therapeutics and marketed under the brand name Filspari. It is used for the treatment of IgA nephropathy and focal segmental glomerulosclerosis (FSGS) (Syed, 2023; Zhang *et al.*, 2020). By blocking the ETA receptor, this drug reduces vasoconstriction, inflammation and fibrosis, while its AT1 receptor antagonism lowers blood pressure and protects kidney function. This dual mechanism is effective for treating kidney diseases, such as focal segmental glomerulosclerosis (FSGS) and IgA nephropathy (IgAN), as proteinuria is reduced and disease progression slowed (Kohan *et al.*, 2024). The SST molecule is highly flexible and contains seven hydrogen-bond acceptors, one hydrogen-bond donor and 12 torsion angles (Murugesan *et al.*, 2002). Its molecular flexibility predisposes sparsentan to the formation of an amorphous phase (Macikenas *et al.*, 2019). An amorphous phase typically dissolves faster than its stable crystalline counterpart, but is generally less stable over time, which can potentially lead to performance variability (Desiraju, 2007). Although limited structural data for this phase have been disclosed (Murugesan *et al.*, 2005), the detailed structural and conformational information which are necessary to understand its properties and behaviour have not been available so far. Therefore, we have carried out a comprehensive crystallographic study to establish the solid-state characteristics of the SST molecule.

Flexible molecules can adopt a range of energetically viable conformations whose specific crystal packing preferences may then result in the formation of polymorphs, *i.e.* a single molecule crystallizes in multiple crystal forms with distinct molecular packing arrangements and physical properties (Tang *et al.*, 2021). The study of flexible molecules is therefore an

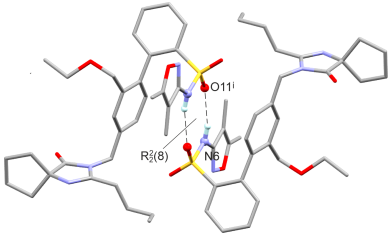

important topic in materials science, pharmaceutical research and crystal engineering. In addition, molecular flexibility may also be linked with the observation of structural disorder in certain crystals. Many molecular crystals and more than 20% of the crystal structures deposited in the Cambridge Structural Database (CSD) exhibit some form of disorder (Groom *et al.*, 2016; Linden, 2023). The accurate refinement of these structures depends critically on the available diffraction data, as only high-quality data enable a reliable determination of the molecular geometry and a sufficient resolution of the disordered regions, and weak data will lead to inferior results (Diederichs, 2016). In this context, energy calculations that are aimed at identifying the energetically most favourable conformations within the lattice have become a valuable tool for a more reliable disorder refinement. For instance, energy minimization techniques like the 'molecule-in-cluster' approach allow the analysis of each of the possible molecular conformations within its crystal environment, refining the model based on the most stable conformations (Dittrich, 2021). By computationally optimizing each molecular arrangement and applying targeted restraints, the alignment between the model and the experimental data is improved, and thus the accuracy and precision of disorder refinement in structural analysis is enhanced (Müller, 2021). In the present study, the crystal structure refinement revealed multiple disordered fragments within the SST molecule. Advanced techniques, including energy calculations (Clark *et al.*, 2005), were applied to assess the viability of alternative disorder geometries and also to evaluate which of these are likely to co-exist in individual molecules.

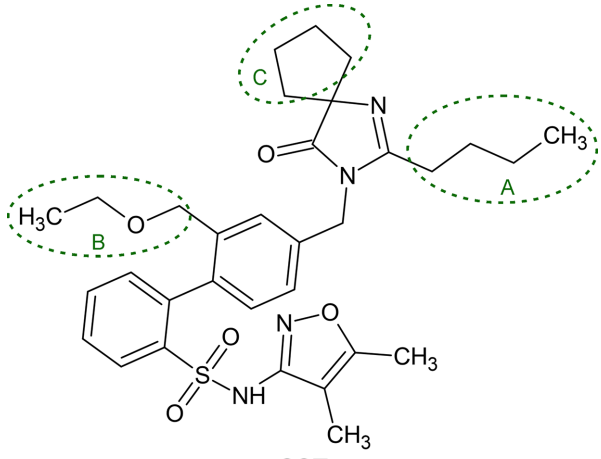

SST
Scheme 1

2. Experimental

2.1. Materials

Amorphous SST was obtained from Taros Chemicals. This substance was recrystallized prior to use in further experiments (details of the recrystallization method are provided below). Analytical grade solvents were procured from commercial suppliers.

Table 1
Experimental details.

Crystal data	
Chemical formula	$C_{32}H_{40}N_4O_5S$
M_r	592.74
Crystal system, space group	Triclinic, $P\overline{1}$
Temperature (K)	193
a, b, c (Å)	11.3363 (10), 11.8815 (8), 14.0763 (10)
α, β, γ (°)	98.113 (6), 112.679 (8), 110.711 (7)
V (Å^3)	1549.4 (2)
Z	2
Radiation type	Mo $K\alpha$
μ (mm^{-1})	0.15
Crystal size (mm)	0.25 × 0.25 × 0.15
Data collection	
Diffractometer	Rigaku Xcalibur Gemini ultra diffractometer with a Ruby detector
Absorption correction	Multi-scan (*CrysAlis PRO*; Rigaku OD, 2020)
T_{min}, T_{max}	0.921, 1.000
No. of measured, independent and observed [$I > 2\sigma(I)$] reflections	14469, 6837, 4250
R_{int}	0.042
(sin $\theta/\lambda)_{max}$ (Å^{-1})	0.641
Refinement	
$R[F^2 > 2\sigma(F^2)]$, $wR(F^2)$, S	0.054, 0.140, 1.03
No. of reflections	6837
No. of parameters	528
No. of restraints	483
H-atom treatment	H atoms treated by a mixture of independent and constrained refinement
$\Delta\rho_{max}$, $\Delta\rho_{min}$ (e Å^{-3})	0.48, −0.31

Computer programs: *CrysAlis PRO* (Rigaku OD, 2020), *SHELXT* (Sheldrick, 2015*a*), *SHELXL2014* (Sheldrick, 2015*b*) and *XP* (Bruker, 1998).

2.2. Preparation of crystalline SST

Amorphous SST (1 g) was dissolved in 5 ml of isopropanol and 5 ml of water was added dropwise to the mixture. The resulting mixture was then warmed to 40 °C to produce a clear solution. This solution was allowed to cool and kept at room temperature, resulting in the formation of white prismatic crystals suitable for single-crystal structure determination. These crystals were filtered off, washed with a small amount of a 2:1 isopropanol–water mixture and dried to yield a white crystalline solid.

2.3. Single-crystal structure refinement

Crystal data, data collection and structure refinement details are summarized in Table 1. All H atoms, except for those in disordered fragments, were identified in difference maps. Methyl H atoms were idealized and included as rigid groups allowed to rotate but not tip (C—H = 0.98 Å), with U_{iso}(H) parameters set to 1.5U_{eq}(C) of the parent atom. H atoms bonded to secondary CH_2 and tertiary CH atoms (C—H = 0.99 Å), and H atoms in aromatic groups (C—H = 0.95 Å) were positioned geometrically, with U_{iso}(H) values set to 1.2U_{eq}(C) of the parent atom. The H atom of the NH group was refined with a restrained bond length [N6—H6 = 0.88 (1) Å] and its U_{iso}(H) parameter was refined freely.

Several sections of the SST molecule were found to exhibit positional disorder, *i.e.* the butyl group (–C39—C40—C41—C42; labelled **A** in Scheme 1), the ethoxymethyl group (–C24—O25—C26—C27; labelled **B**) and the cyclopentyl ring (C34–C37; labelled **C**). A combination of restraints on chemically equivalent 1,2- and 1,3-distances, and restraints on anisotropic displacement parameters was applied in the refinement of the non-H-atom positions in the disordered parts of the molecules. The refined final occupancies were **A1**/**A2** = 0.804 (5):0.196 (5), **B1**/**B2**/**B3** = 0.597 (3):0.223 (3):0.180 (2) and **C1**/**C2** = 0.571 (18):0.429 (18). A detailed description of the disorder model is given in Section 3.2 below.

2.4. Periodic electronic structure calculations

Six ordered structure models based on the disorder fragments in sections **A** and **B** of the SST molecule (Scheme 1) were generated. These models represented the initial configurations for periodic electronic structure optimization using *CASTEP* (Version 23.1; Clark *et al.*, 2005) to generate optimized atomic positions and lattice parameters. The Perdew–Burke–Ernzerhof (PBE) generalized gradient approximation (GGA) exchange-correlation density functional (Perdew *et al.*, 1996) was applied, along with ultrasoft pseudopotentials (Vanderbilt, 1990) and the MBD* semi-empirical dispersion correction (Tkatchenko *et al.*, 2012). The *k*-point grid was chosen to maintain a maximum spacing of $2\pi \times 0.07$ Å^{-1}, with a basis set cut-off energy of 780 eV. Convergence criteria were set to an energy precision better than 2×10^{-5} eV per atom, atomic displacements within 1×10^{-3}, maximum forces below 1×10^{-3} Å and maximum stresses below 0.1 GPa. The main component of the cyclopentyl ring (section **C** in Scheme 1) was used for all models, as the calculations were carried out to investigate the disordered chain conformations.

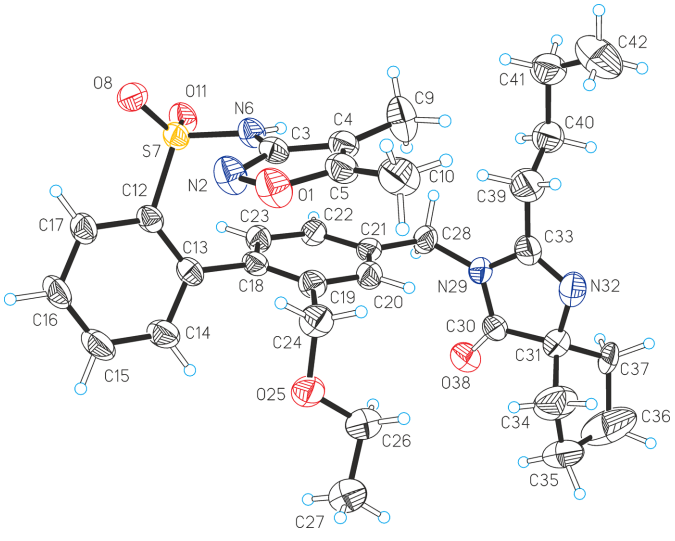

Figure 1
The molecular structure of SST, with displacement ellipsoids drawn at the 50% probability level and H atoms drawn as spheres of arbitrary size (minor disorder has been omitted for clarity).

2.5. Pairwise intermolecular energy calculations

CrystalExplorer (Version 17; Mackenzie *et al.*, 2017; Spackman *et al.*, 2021) and *GAUSSIAN16* (Frisch *et al.*, 2019) were used to calculate the pairwise intermolecular energies for the PBE-MBD*-generated structure models of SST within a 3.80 Å radius, using the B3LYP/6-31G(d,p) wavefunction.

3. Results and discussion

3.1. Molecular geometry and hydrogen bonding

The asymmetric unit contains a single SST molecule (Fig. 1). The C12—C13—C18—C23 torsion angle, corresponding to the twist between the two central arene rings, is −69.7 (3)°. The C28—N29 bond is slightly out of the mean plane formed by atom C28 and the adjacent arene ring [C20—C21—C28—N29 = 14.6 (3)°], and the angle between the latter mean plane and that defined by atom C28 and the neighbouring imidazole ring (N29/C30/C31/N32/C33) is 82.33 (8)°. In the *N*-(1,2-oxazol-3-yl)benzenesulfonamide fragment, the N2—C3 bond of the oxazole ring and the S7—C12 bond adopt a *cis* arrangement, and the central C3—N6—S7—C12 chain displays a *gauche* conformation, corresponding to values of 3.2 (3), −60.5 (2) and −41.7 (2)° for the three essential torsion angles N2—C3—N6—S7 (τ_1), C3—N6—S7—C12 (τ_2) and N6—S7—C12—C13 (τ_3). The most recent version of the Cambridge Structural Database (CSD, Version 6.00; Groom *et al.*, 2016) contains another 67 examples of the same molecular fragment in 55 different crystal structures, and the values of the torsion angles τ_1–τ_3 (Fig. 2, inset) were collected for each of these examples (Table S1 of the supporting information). As

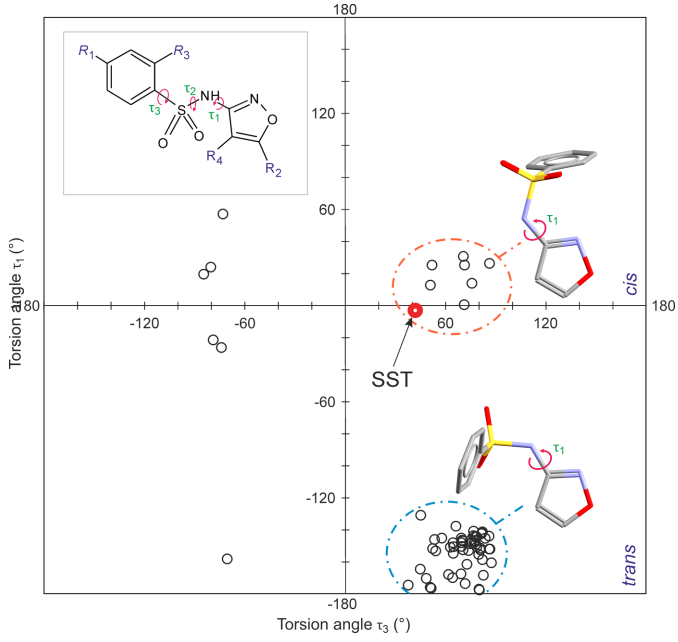

Figure 2
Survey of the experimental conformations of the *N*-(1,2-oxazol-3-yl)-benzenesulfonamide fragment characterized by torsion angles τ_1–τ_3 (inset). The τ_3 *versus* τ_1 plot shows two clusters which correspond to preferred conformations.

Table 2
Hydrogen-bond geometry (Å, °).

D—H···A	D—H	H···A	D···A	D—H···A
N6—H6···O11^{i}	0.88 (1)	2.12 (1)	2.951 (2)	159 (2)
C28—H28A···O38^{ii}	0.99	2.40	3.318 (3)	153
C28—H28B···O8^{i}	0.99	2.46	3.265 (3)	138

Symmetry codes: (i) $-x+1, -y+1, -z+1$; (ii) $-x+2, -y+2, -z+1$.

two inversion-equivalent sets of torsions are present in each of these structures, the values of τ_1, τ_2 and τ_3 were normalized so that $\tau_2 \geq 0°$ in order to facilitate a meaningful comparison. The obtained geometrical parameters are listed in Table S1 of the supporting information. All values for the central angle τ_2 lie within a narrow range between 50.1 and 86.1°, *i.e.* the central C—N—S—C chain is always *gauche* and its conformational flexibility is small. Moreover, a plot of τ_1 values against τ_3 angles reveals two distinct densely populated clusters of data points in the narrow range $41.7 \leq \tau_3 \leq 86.5°$. The corresponding τ_1 values approach 180° in the first cluster (encircled in blue in Fig. 2), indicating a *trans* orientation of the S—C bond relative to the N—C bond of the oxazole ring. By contrast, τ_1 values are close to 0° in the second cluster (encircled in red in Fig. 2), which corresponds to a *cis* conformation and also contains the data point for SST. Therefore, the τ_1 torsion describes a section of the molecule which is typically planar and gives rise to two distinct geometries which are related by a 180° rotation about the central N—C bond.

The SST molecule contains seven potential acceptor sites for hydrogen bonds and one hydrogen-bond donor group, *i.e.* the NH group of the sulfonamide fragment. The latter forms an N6—H6···O11^{i} interaction with a sulfonyl O atom of a neighbouring molecule (see Table 2 for symmetry codes). The resulting centrosymmetric dimer (Fig. 3) displays an $R_2^2(6)$ ring (Etter *et al.*, 1990; Bernstein *et al.*, 1995). Within this dimer, there is also a short intermolecular contact, C28—H28B···O8^{i}, with an H···O separation of 2.46 Å, which involves the second sulfonyl O atom and the CH_2 group linking the substituted imidazole ring with the arene ring (Table 2). The same CH_2 group is additionally engaged in a significant interaction with the carbonyl group of a third molecule, C28—H28A···O38^{ii}, where the H···O distance is 2.40 Å.

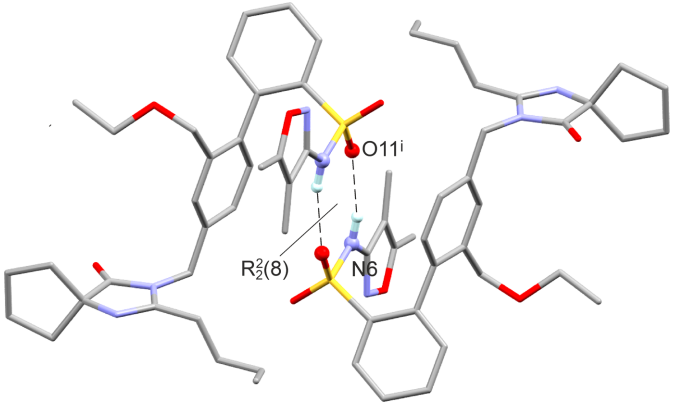

Figure 3
N—H···O hydrogen-bonded dimer (minor disorder and H atoms bonded to C atoms have been omitted for clarity). [Symmetry code: (i) $-x+1$, $-y+1$, $-z+1$.]

3.2. Disorder model

In the case of the disordered **B** chain, the initial refinement was also carried out with a two-component model. The resulting disordered chain geometries displayed sensible 1,2- and 1,3-distances. The corresponding occupancy ratio was 0.7:0.3, $R[F^2 > 2\sigma(F^2)] = 0.066$ and $wR(F^2) = 0.205$. However, this model displayed some unusual features, especially with regard to the position of the C27′ methyl group of the minor component (see Fig. S6 of the supporting information). In addition to an unexpected large spatial separation between alternative methyl-group positions (C27···C27′ = 1.94 Å), the C27′ methyl group was in close proximity to the C18–C23 ring of a second molecule with C27′···C23^{iii} = 2.63 Å [symmetry code: (iii) $-x+1, -y+2, -z+1$], resulting in several atypically short intermolecular distances. This situation could not be improved by the application of anti-bumping restraints. Moreover, the region of the disordered **B** chain also contained significant residual electron-density peaks, with $\Delta\rho_{max}$ = 1.02 e Å^{-3} at a distance of 2.64 Å from C23^{iii}.

Additionally, energy calculations carried out on the four theoretical ordered crystal structures containing optimized molecular geometries representing possible **A**/**B** combinations

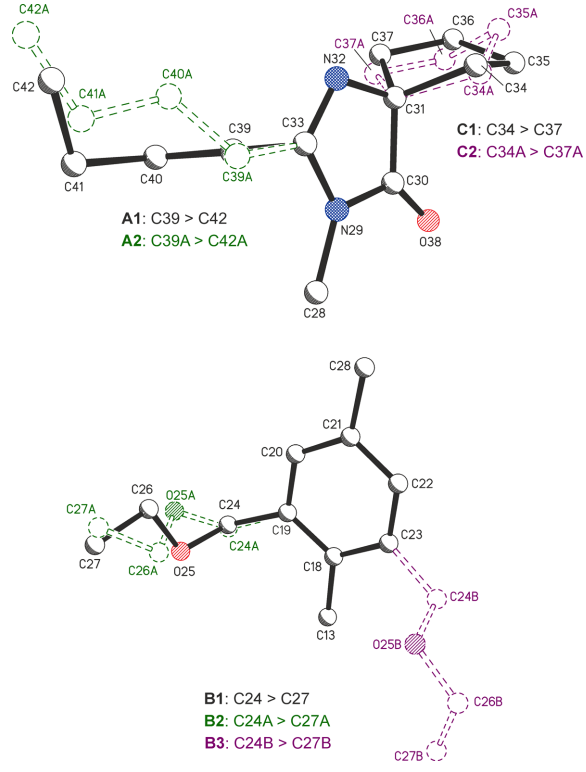

Figure 4
Detailed views of the alternative chain conformations of the disorder components **A1**/**A2** and **C1**/**C2** (top), and **B1**/**B2**/**B3** (bottom; H atoms have been omitted for clarity).

indicated a significant disadvantage associated with the minor **B** component (see Fig. S7 of the supporting information).

The search for a better model then let us consider the possibility of a third disorder component **B3** of the chain (–C24—O25—C26—C27), which results from the rotation of the arene ring about the C13—C18···C21—C28 axis by approximately 180° (see Fig. 4). The geometry of the first disorder component **B1** was largely unchanged in this new three-way-split model. The main difference between **B1** and the second component **B2** is a 44° rotation about the C19—C24 bond (see Table S8 of the supporting information). As expected, the alternative positions of the two methyl groups lie in very close proximity, *i.e.* C27···C27*A* = 0.371 (16) Å. The final occupancies of **B1**, **B2** and **B3** were 0.597 (3), 0.223 (3) and 0.180 (2), respectively. The presence of a **B3** chain in a given molecule means that a particular neighbouring molecule to which it is related by the inversion operation ($-x+1$, $-y+2$, $-z+1$) must also contain the **B3** conformation, *i.e.* the **B3** geometry of one molecule is geometrically incompatible with a **B1** or **B2** chain in the other. The refined site occupancy of 0.804 for the major **A1** component is similar to the sum of the occupancies of 0.820 for **B1** and **B2**, but it cannot be ascertained from diffraction data how the occupancies in sections **A** and **B** of the SST molecule are correlated with one another. This topic was investigated further with energy calculations, discussed in the following section, which were also used to establish the viability of the obtained chain conformations.

The conformations **C1** and **C2** of the disordered cyclopentyl ring were analysed using *PLATON* (Spek, 2020). Ring-puckering parameters (Cremer & Pople, 1975) of q = 0.421 (13) Å and ϕ = 28 (2)° obtained for the major component indicate an intermediate geometry between C34-envelope and C31/C34-twist. The minor component (Fig. 4) displays a conformation between C36*A*-envelope and C36*A*/C35*A*-twist, resulting in ring-puckering parameters of q = 0.338 (19) Å and ϕ = 279 (3)°.

3.3. Energy calculations

To further investigate the disorder in the $-CH_2CH_2CH_2CH_3$ (section **A** in Scheme 1) and $-CH_2OCH_2CH_3$ (section **B**) groups, six independent ordered structural models were generated, each starting from one of the disorder sites identified in the experimental structure. These structures were then optimized (PBE-MBD*), with the experimental lattice parameters and atomic positions allowed to minimize. The minimizations revealed that the six initial models did not converge to a single structure. Instead, each of the possible positions for both disordered groups yielded a unique minimum on the lattice energy landscape, indicating that the disorder in the **A** group is not linked to the disorder in the **B** group, and *vice versa*. Each of the positions of the **A** and **B** groups was well reproduced in the PBE-MBD* structures, as shown by the overlay of experimental and PBE-MBD* conformations (Fig. 5).

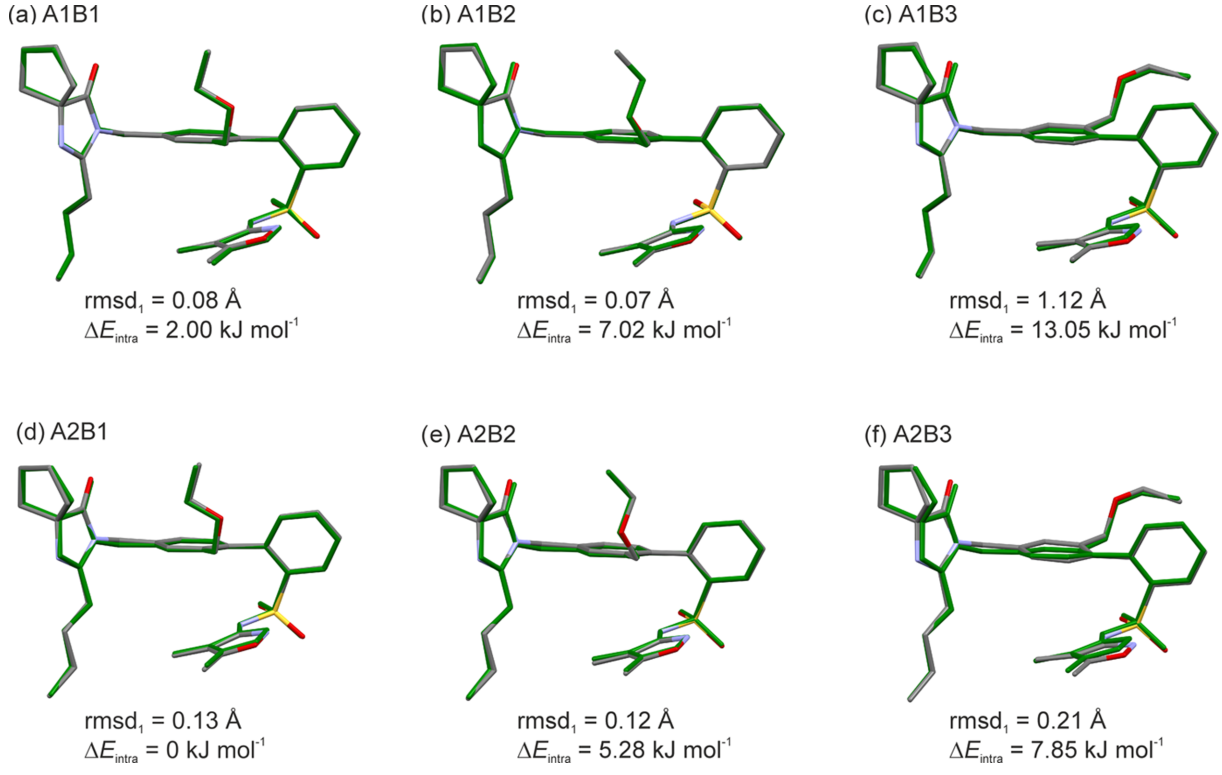

Figure 5
Overlay of the experimental conformations (coloured by element) with the conformations observed in the optimized structures (in green). Rmsd$_1$ and intramolecular energy differences (ΔE_{intra}) were calculated at the B3LYP/6-31G(d,p) level of theory. ΔE_{intra} values are reported relative to the lowest energy among the six conformations.

Table 3
Lattice energy differences (PBE-MBD*, kJ mol^{-1}) among the six ordered STU structure models and rmsd$_{15}$ values (Å).

Structure	ΔE_{latt}	rmsd$_{15}$	Structure	ΔE_{latt}	rmsd$_{15}$
A1B1	0.00	0.15	**A2B1**	7.23	0.24
A1B2	6.45	0.12	**A2B2**	11.67	0.18
A1B3	6.01	0.39	**A2B3**	8.88	0.39

The intramolecular energy differences (ΔE_{intra}) for the six conformations were estimated at the B3LYP/6-31G(d,p) level of theory. **A2B1** was identified as the lowest-energy conformation among the six (calculated in the gas phase), although it was only 2.00 kJ mol^{-1} lower than **A1B1**. Therefore, the energy difference between the two **A** chain orientations is relatively small compared to the energy differences between the **B** orientations, which were estimated to be in the range 5–11 kJ mol^{-1}.

Less favourable intramolecular energies can be offset by stronger intermolecular interactions within the crystal structure. A comparison of the lattice energies (PBE-MBD*) of the six distinct orientations (Table 3) in the SST structure revealed that the three structures adopting the **A1** orientation are lower in energy than the three **A2**-based structures. In the experimental structure, the disorder ratio was refined to 0.45:0.55, with **A2** being only slightly favoured. Adding the **B** orientations to the comparison revealed that **B1** is favoured over **B2** and **B3**, which is clearly reflected in the disorder ratio of 0.60 for **B1**, compared to 0.22 and 0.18 for the remaining two orientations. Overall, the structure optimizations revealed that **A1B1** might be the most stable of the six models based on lattice energy calculations. However, with the exception of the **A2B2** model, all are within 10 kJ mol^{-1}. The calculations demonstrate that numerous orientations are feasible for forming low-energy structures, and adding entropic contributions is expected to further stabilize the structures. This helps rationalize the high tendency toward disorder in the SST structure. All orientations were well reproduced in the models, with the **B3** orientation, a minor orientation involving a 180° flip of the biphenyl Ph–Ph dihedral, showing a slightly higher rmds$_{15}$ value than the other structures (Table 3).

In addition to calculating the lattice energy differences between the models, we also computed the pairwise intermolecular interaction energies for the PBE-MBD* structures. The six optimized structure models exhibit identical packing arrangements (Fig. 6), differing only in the torsional variations of the two flexible groups. The $R_2^2(8)$ dimer motif was identi-

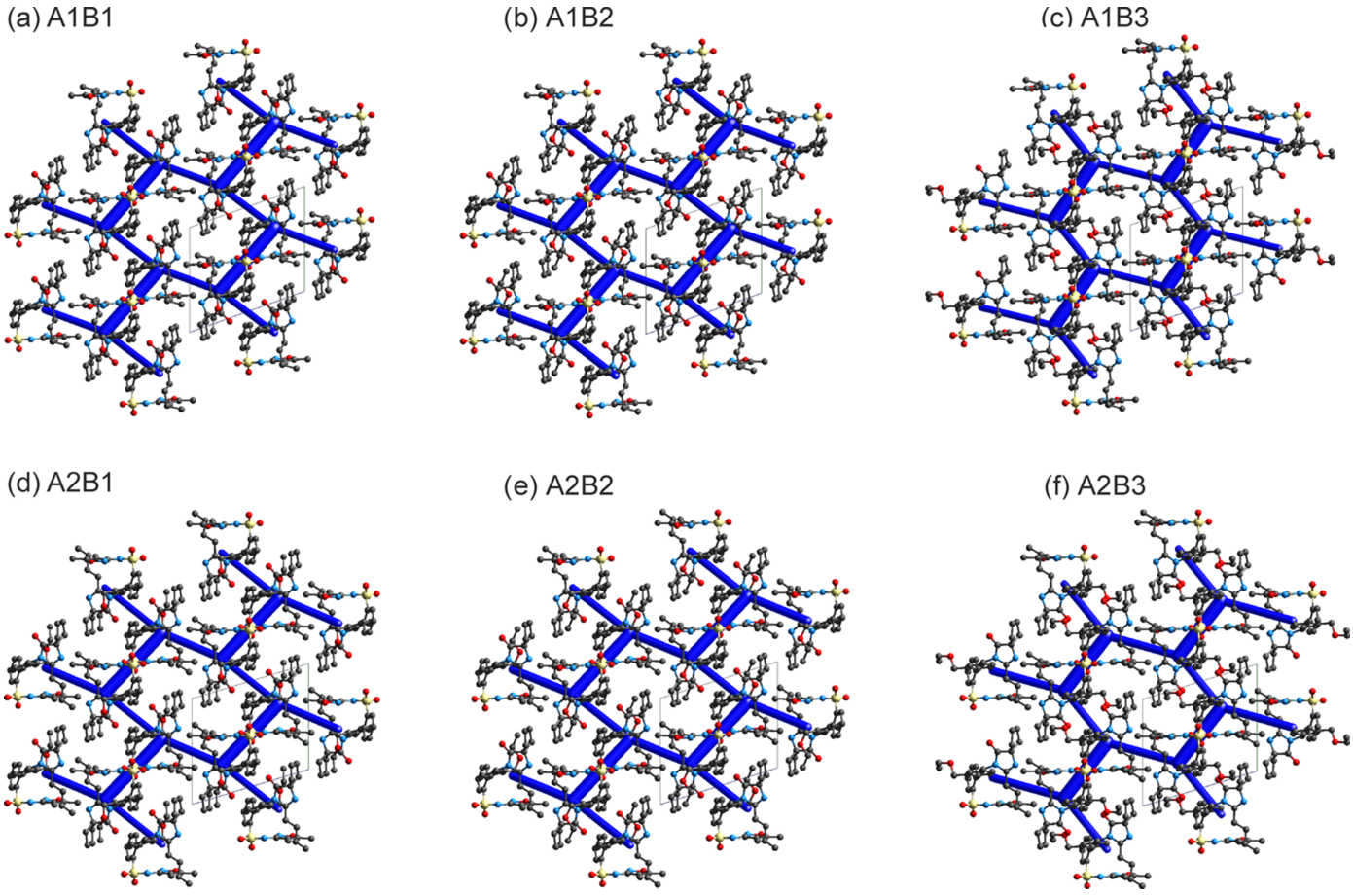

Figure 6
Energy framework diagrams (total energy), illustrating that all six tested sparsentan models result in the same order of the strong pairwise interactions. The energy scale factor is 50. Stabilizing contacts are shown in blue and the thickness corresponds to the strength. Pairwise interaction energies less than 20 kJ mol^{-1} and H atoms have been omitted for clarity. The packing diagrams are displayed along the respective crystallographic *a* axes.

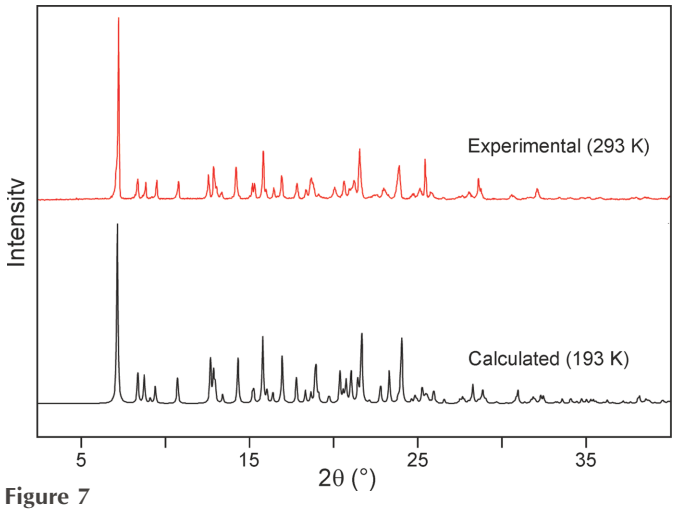

Figure 7
Experimental PXRD pattern of SST (top) and a simulated pattern derived from the single-crystal structure (bottom).

fied as the strongest pairwise intermolecular interaction, with an interaction energy between −127.8 and −150.1 kJ mol^{-1}. This interaction is stabilized not only by significant electrostatic contributions but also by dispersion forces. Sparsentan, which has a single hydrogen-bond donor group, but multiple aromatic rings and flexible alkyl chains, allows for the formation of relatively strong aromatic interactions and close contacts. The second and third strongest interactions fall within the −92.5 to −72.9 kJ mol^{-1} range (Tables S3–S6 of the supporting information) and, despite their strength, they do not involve classical strong hydrogen bonds, highlighting the crucial role of dispersion forces in stabilizing the crystal lattice. The fact that each of the six models remained at a local minimum without transitioning to another arrangement suggests a potential for disorder, often seen in computed crystal energy landscapes where major and minor components appear as separate structures (Hunnisett *et al.*, 2024). The applied lattice energy minimization models do not account for entropic contributions, which are expected to stabilize the structure and, therefore, support the experimentally observed disorder.

3.4. Characterization of the crystalline phase of SST

3.4.1. Powder X-ray diffraction (PXRD)

The experimental room-temperature PXRD pattern of a sample of SST obtained *via* cooling crystallization from acetonitrile matches a corresponding pattern (193 K) calculated with *Mercury* (Macrae *et al.*, 2020) from the crystal structure data (Fig. 7). Slight differences in peak positions are due to different temperature conditions.

3.4.2. Thermal analysis

To investigate the thermal properties of the title compound, including its glass transition temperature (T_g), the differential scanning calorimetry (DSC) analysis was performed as a heating–cooling–heating cycle. The transition temperature T_g was determined using a melt–quench technique. The material was first heated beyond its melting point and then cooled rapidly to trap the molten state in an amorphous form. The DSC plot (Fig. 8, first curve) shows a sharp endothermic peak at 140.6 ± 0.2 °C (onset), which corresponds to the melting of SST, and the TGA thermogram (Fig. 8) shows a concurrent mass loss of 0.60% between 25 and 145 °C. Following the first heating, the amorphous sample was cooled to −20 °C and then reheated to 155 °C, and during this step, the glass transition was observed at T_g = 41.5 °C. This relatively low T_g is indicative of the poor physical stability of amorphous SST and a likelihood of recrystallization from the amorphous state during long-term storage.

3.4.3. FT–IR spectroscopy

The FT–IR spectra (Fig. 9) of the amorphous and the crystalline forms of SST were recorded and compared. In the

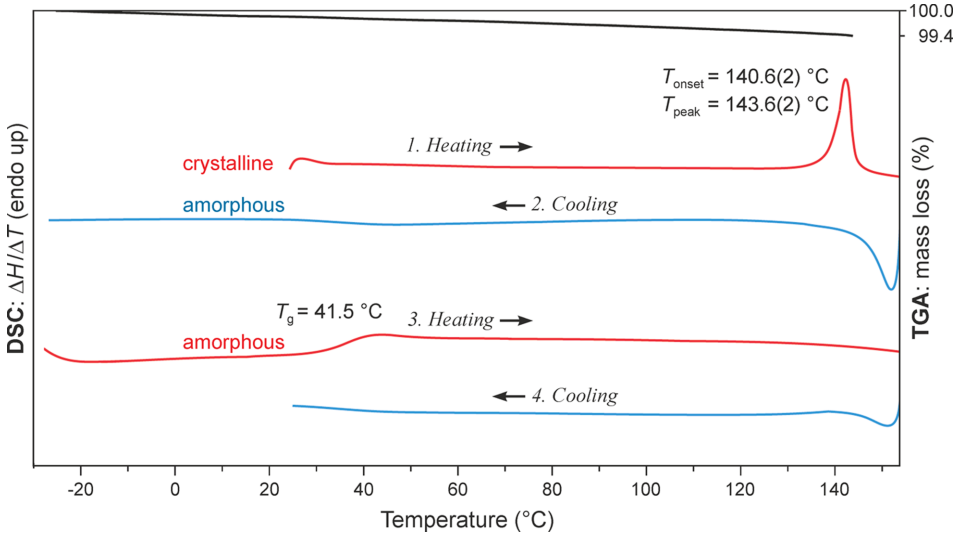

Figure 8
DSC curves: two heating/cooling cycles (red/blue; T_g = glass transition temperature) and the TGA curve (black) of crystalline sparsentan.

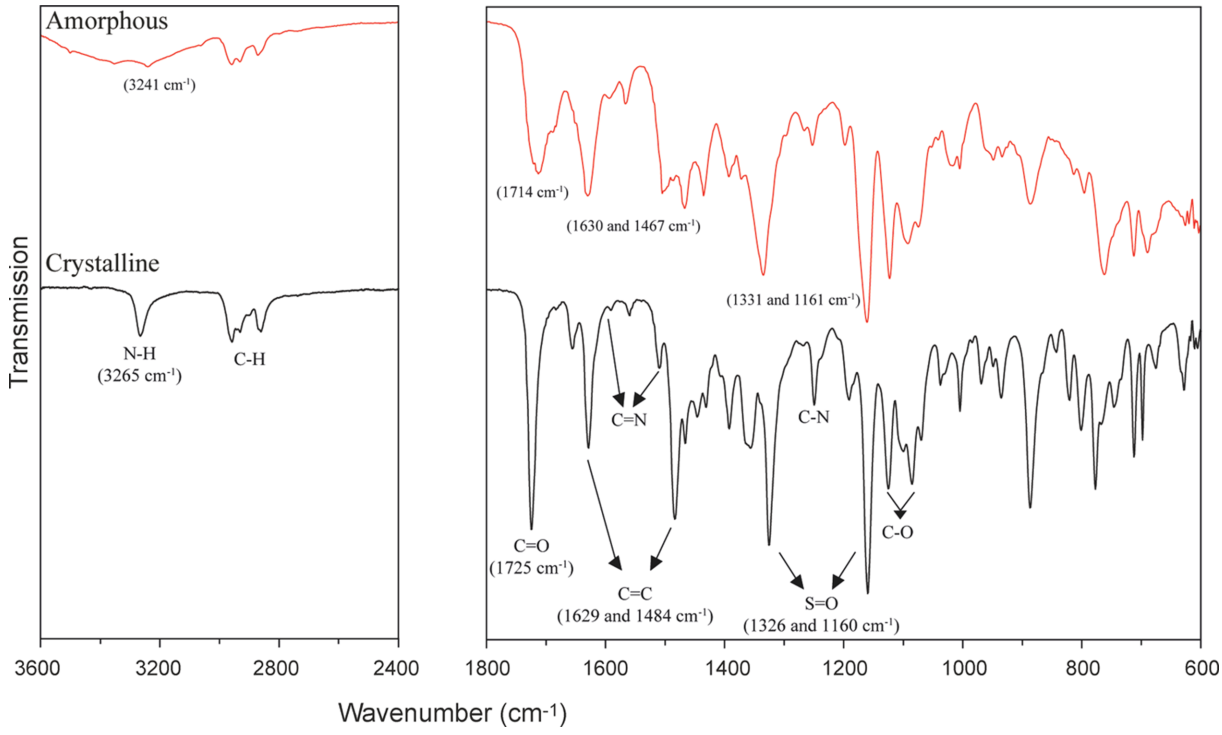

Figure 9
FT–IR spectra of the amorphous (red) and crystalline (black) forms of SST with assigned band positions.

case of the crystalline form, sharp peaks were observed at 1725 (C═O), 1629 and 1484 (C═C), and 1326 and 1160 cm^{-1} (O═S═O). In the spectrum of the amorphous form, the corresponding peak positions are shifted by less than 20 cm^{-1} to lower or higher wavenumbers. Additionally, the crystalline form produces a sharp N—H stretching peak above 3000 cm^{-1}, whilst the corresponding peak in the spectrum of the amorphous form is significantly broadened. This broadening and shifting of peaks is attributed to molecular rearrangements during the amorphization process which disrupt the periodic order of the crystal lattice in the solid state (Moinuddin *et al.*, 2020).

4. Conclusions

In the solid state, the sparsentan molecule exhibits two disordered chain sections (**A** and **B**), in addition to a disordered cyclopentyl ring (section **C**). This study demonstrates the application of complementary energy calculations to improve and interpret a complex disorder model. It was found that an initial disorder model for section **B** contained a minor-occupancy component with an unviable chain geometry. This led to the establishment of an alternative three-component disorder model for **B**, resulting in significantly improved structure refinement parameters. Energy calculations confirmed the viability of the three chain geometries implied by the final model for section **B**. In addition, these computations indicated that the two disordered chains of sections **A** and **B** of the molecule are uncorrelated with regard to their occupancy.

Acknowledgements

The financial support received for the Christian Doppler Laboratory for Advanced Crystal Engineering Strategies in Drug Development by the Austrian Federal Ministry of Economy, Energy and Tourism, the National Foundation for Research, Technology and Development and the Christian Doppler Research Association (award to Doris E. Braun) is gratefully acknowledged. Computational results presented here have been achieved using the LEO HPC infrastructure of the University of Innsbruck.

References

Bernstein, J., Davis, R. E., Shimoni, L. & Chang, N.-L. (1995). *Angew. Chem. Int. Ed. Engl.* **34**, 1555–1573.
Bruker (1998). *XP*. Bruker AXS Inc., Madison, Wisconsin, USA.
Clark, S. J., Segall, M. D., Pickard, C. J., Hasnip, P. J., Probert, M. I. J., Refson, K. & Payne, M. C. (2005). *Z. Kristallogr.* **220**, 567–570.
Cremer, D. & Pople, J. A. (1975). *J. Am. Chem. Soc.* **97**, 1354–1358.
Desiraju, G. R. (2007). *Angew. Chem. Int. Ed.* **46**, 8342–8356.
Diederichs, K. (2016). *Methods Mol. Biol.* **1320**, 147–173.
Dittrich, B. (2021). *IUCrJ* **8**, 305–318.
Etter, M. C., MacDonald, J. C. & Bernstein, J. (1990). *Acta Cryst.* B**46**, 256–262.
Frisch, M. J., Trucks, G. W., Schlegel, H. B., Scuseria, G. E., Robb, M. A., Cheeseman, J. R., Scalmani, G., Barone, V., Petersson, G. A., Nakatsuji, H., Li, X., Caricato, M., Marenich, A. V., Bloino, J., Janesko, B. G., Gomperts, R., Mennucci, B., Hratchian, H. P., Ortiz, J. V., Izmaylov, A. F., Sonnenberg, J. L., Williams-Young, D., Ding, F., Lipparini, F., Egidi, F., Goings, J., Peng, B., Petrone, A., Henderson, T., Ranasinghe, D., Zakrzewski, V. G., Gao, J., Rega, N., Zheng, G., Liang, W., Hada, M., Ehara, M., Toyota, K., Fukuda, R.,

Hasegawa, J., Ishida, M., Nakajima, T., Honda, Y., Kitao, O., Nakai, H., Vreven, T., Throssell, K., Montgomery, J. A. J., Peralta, J. E., Ogliaro, F., Bearpark, M. J., Heyd, J. J., Brothers, E. N., Kudin, K. N., Staroverov, V. N., Keith, T. A., Kobayashi, R., Normand, J., Raghavachari, K., Rendell, A. P., Burant, J. C., Iyengar, S. S., Tomasi, J., Cossi, M., Millam, J. M., Klene, M., Adamo, C., Cammi, R., Ochterski, J. W., Martin, R. L., Morokuma, K., Farkas, O., Foresman, J. B. & Fox, D. J. (2019). *GAUSSIAN16*. Revision C.01. Gaussian Inc., Wallingford, CT, USA. https://gaussian.com/.

Groom, C. R., Bruno, I. J., Lightfoot, M. P. & Ward, S. C. (2016). *Acta Cryst.* B**72**, 171–179.

Hunnisett, L. M., Francia, N., Nyman, J., Abraham, N. S., Aitipamula, S., Alkhidir, T., Almehairbi, M., Anelli, A., Anstine, D. M., Anthony, J. E., Arnold, J. E., Bahrami, F., Bellucci, M. A., Beran, G. J. O., Bhardwaj, R. M., Bianco, R., Bis, J. A., Boese, A. D., Bramley, J., Braun, D. E., Butler, P. W. V., Cadden, J., Carino, S., Červinka, C., Chan, E. J., Chang, C., Clarke, S. M., Coles, S. J., Cook, C. J., Cooper, R. I., Darden, T., Day, G. M., Deng, W., Dietrich, H., DiPasquale, A., Dhokale, B., van Eijck, B. P., Elsegood, M. R. J., Firaha, D., Fu, W., Fukuzawa, K., Galanakis, N., Goto, H., Greenwell, C., Guo, R., Harter, J., Helfferich, J., Hoja, J., Hone, J., Hong, R., Hušák, M., Ikabata, Y., Isayev, O., Ishaque, O., Jain, V., Jin, Y., Jing, A., Johnson, E. R., Jones, I., Jose, K. V. J., Kabova, E. A., Keates, A., Kelly, P. F., Klimeš, J., Kostková, V., Li, H., Lin, X., List, A., Liu, C., Liu, Y. M., Liu, Z., Lončarić, I., Lubach, J. W., Ludík, J., Marom, N., Matsui, H., Mattei, A., Mayo, R. A., Melkumov, J. W., Mladineo, B., Mohamed, S., Momenzadeh Abardeh, Z., Muddana, H. S., Nakayama, N., Nayal, K. S., Neumann, M. A., Nikhar, R., Obata, S., O'Connor, D., Oganov, A. R., Okuwaki, K., Otero-de-la-Roza, A., Parkin, S., Parunov, A., Podeszwa, R., Price, A. J. A., Price, L. S., Price, S. L., Probert, M. R., Pulido, A., Ramteke, G. R., Rehman, A. U., Reutzel-Edens, S. M., Rogal, J., Ross, M. J., Rumson, A. F., Sadiq, G., Saeed, Z. M., Salimi, A., Sasikumar, K., Sekharan, S., Shankland, K., Shi, B., Shi, X., Shinohara, K., Skillman, A. G., Song, H., Strasser, N., van de Streek, J., Sugden, I. J., Sun, G., Szalewicz, K., Tan, L., Tang, K., Tarczynski, F., Taylor, C. R., Tkatchenko, A., Tom, R., Touš, P., Tuckerman, M. E., Unzueta, P. A., Utsumi, Y., Vogt-Maranto, L., Weatherston, J., Wilkinson, L. J., Willacy, R. D., Wojtas, L., Woollam, G. R., Yang, Y., Yang, Z., Yonemochi, E., Yue, X., Zeng, Q., Zhou, T., Zhou, Y., Zubatyuk, R. & Cole, J. C. (2024). *Acta Cryst.* B**80**, 548–574.

Kohan, D. E., Bedard, P. W., Jenkinson, C., Hendry, B. & Komers, R. (2024). *Clin. Sci.* **138**, 645–662.

Linden, A. (2023). *Acta Cryst.* C**79**, 69–70.

Macikenas, D., Ruby, K., Hulvat, J. F. & Wu, X. (2019). Int. Patent Appl. WO2020132594A1.

Mackenzie, C. F., Spackman, P. R., Jayatilaka, D. & Spackman, M. A. (2017). *IUCrJ* **4**, 575–587.

Macrae, C. F., Sovago, I., Cottrell, S. J., Galek, P. T. A., McCabe, P., Pidcock, E., Platings, M., Shields, G. P., Stevens, J. S., Towler, M. & Wood, P. A. (2020). *J. Appl. Cryst.* **53**, 226–235.

Moinuddin, S. M., Shi, Q., Tao, J., Guo, M., Zhang, J., Xue, Q., Ruan, S. & Cai, T. (2020). *AAPS PharmSciTech* **21**, 41.

Müller, P. (2021). *IUCrJ* **8**, 150–151.

Murugesan, N., Gu, Z., Fadnis, L., Tellew, J. E., Baska, R. A. F., Yang, Y., Beyer, S. M., Monshizadegan, H., Dickinson, K. E., Valentine, M. T., Humphreys, W. G., Lan, S.-J., Ewing, W. R., Carlson, K. E., Kowala, M. C., Zahler, R. & Macor, J. E. (2005). *J. Med. Chem.* **48**, 171–179.

Murugesan, N., Tellew, J. E., Gu, Z., Kunst, B. L., Fadnis, L., Cornelius, L. A., Baska, R. A. F., Yang, Y., Beyer, S. M., Monshizadegan, H., Dickinson, K. E., Panchal, B., Valentine, M. T., Chong, S., Morrison, R. A., Carlson, K. E., Powell, J. R., Moreland, S., Barrish, J. C., Kowala, M. C. & Macor, J. E. (2002). *J. Med. Chem.* **45**, 3829–3835.

Perdew, J. P., Burke, K. & Ernzerhof, M. (1996). *Phys. Rev. Lett.* **77**, 3865–3868.

Rigaku OD (2020). *CrysAlis PRO*. Rigaku Oxford Diffraction Ltd, Yarnton, Oxfordashire, England.

Sheldrick, G. M. (2015*a*). *Acta Cryst.* A**71**, 3–8.

Sheldrick, G. M. (2015*b*). *Acta Cryst.* C**71**, 3–8.

Spackman, P. R., Turner, M. J., McKinnon, J. J., Wolff, S. K., Grimwood, D. J., Jayatilaka, D. & Spackman, M. A. (2021). *J. Appl. Cryst.* **54**, 1006–1011.

Spek, A. L. (2020). *Acta Cryst.* E**76**, 1–11.

Syed, Y. Y. (2023). *Drugs* **83**, 563–568.

Tang, S. K., Davey, R. J., Sacchi, P. & Cruz-Cabeza, A. J. (2021). *Chem. Sci.* **12**, 993–1000.

Tkatchenko, A., Alfè, D. & Kim, K. S. (2012). *J. Chem. Theory Comput.* **8**, 4317–4322.

Vanderbilt, D. (1990). *Phys. Rev. B* **41**, 7892–7895.

Zhang, J., Dziewanowska, Z. E., Belder, R., Henderson, I., Bogardus, J. B. & Zhang, Z. (2020). Eur. Patent Appl. EP3708163(A1).

supporting information

Acta Cryst. (2025). C**81**, 530-538 [https://doi.org/10.1107/S2053229625007181]

The disordered structure of sparsentan: energy calculations for competing chain conformations

Thomas Gelbrich, Kristaps Saršüns and Doris E. Braun

Computing details

2-{4-[(2-Butyl-4-oxo-1,3-diazaspiro[4.4]non-1-en-3-yl)methyl]-2-(ethoxymethyl)phenyl}-*N*-(4,5-dimethyl-1,2-oxazol-3-yl)benzenesulfonamide

Crystal data

$C_{32}H_{40}N_4O_5S$
M_r = 592.74
Triclinic, $P\overline{1}$
a = 11.3363 (10) Å
b = 11.8815 (8) Å
c = 14.0763 (10) Å
α = 98.113 (6)°
β = 112.679 (8)°
γ = 110.711 (7)°
V = 1549.4 (2) Å^3
Z = 2
$F(000)$ = 632
D_x = 1.270 Mg m^{-3}
Mo $K\alpha$ radiation, λ = 0.71073 Å
Cell parameters from 4034 reflections
θ = 2.1–27.5°
μ = 0.15 mm^{-1}
T = 193 K
Block, colourless
0.25 × 0.25 × 0.15 mm

Data collection

Rigaku Xcalibur Gemini ultra diffractometer with a Ruby detector
Radiation source: fine-focus sealed X-ray tube, Enhance (Mo) X-ray Source
Graphite monochromator
Detector resolution: 10.3575 pixels mm^{-1}
ω scans
Absorption correction: multi-scan (CrysAlis PRO; Rigaku OD, 2020)
T_{min} = 0.921, T_{max} = 1.000
14469 measured reflections
6837 independent reflections
4250 reflections with $I > 2\sigma(I)$
R_{int} = 0.042
θ_{max} = 27.1°, θ_{min} = 1.9°
h = −14→13
k = −15→15
l = −17→18

Refinement

Refinement on F^2
Least-squares matrix: full
$R[F^2 > 2\sigma(F^2)]$ = 0.054
$wR(F^2)$ = 0.140
S = 1.03
6837 reflections
528 parameters
483 restraints
Primary atom site location: structure-invariant direct methods
Secondary atom site location: difference Fourier map
Hydrogen site location: mixed
H atoms treated by a mixture of independent and constrained refinement
$w = 1/[\sigma^2(F_o^2) + (0.0559P)^2 + 0.1427P]$ where $P = (F_o^2 + 2F_c^2)/3$
$(\Delta/\sigma)_{max}$ = 0.001
$\Delta\rho_{max}$ = 0.48 e Å^{-3}
$\Delta\rho_{min}$ = −0.31 e Å^{-3}
Extinction correction: SHELXL2014 (Sheldrick, 2015*b*), $Fc^*=kFc[1+0.001xFc^2\lambda^3/\sin(2\theta)]^{-1/4}$
Extinction coefficient: 0.0105 (14)

Special details

Geometry. All esds (except the esd in the dihedral angle between two l.s. planes) are estimated using the full covariance matrix. The cell esds are taken into account individually in the estimation of esds in distances, angles and torsion angles; correlations between esds in cell parameters are only used when they are defined by crystal symmetry. An approximate (isotropic) treatment of cell esds is used for estimating esds involving l.s. planes.

Fractional atomic coordinates and isotropic or equivalent isotropic displacement parameters (Å²)

	x	*y*	*z*	U_{iso}*/U_{eq}	Occ. (<1)
O1	0.00778 (17)	0.41650 (17)	0.14189 (13)	0.0480 (5)	
N2	0.0841 (2)	0.4553 (2)	0.25702 (15)	0.0449 (5)	
C3	0.2017 (2)	0.4463 (2)	0.27558 (17)	0.0324 (5)	
C4	0.2117 (2)	0.4057 (2)	0.18051 (18)	0.0349 (5)	
C5	0.0865 (2)	0.3879 (2)	0.10009 (18)	0.0392 (6)	
N6	0.30571 (19)	0.47637 (18)	0.38134 (14)	0.0334 (4)	
H6	0.3925 (14)	0.491 (2)	0.394 (2)	0.053 (8)*	
S7	0.29254 (6)	0.51760 (5)	0.49058 (4)	0.03276 (17)	
O8	0.16728 (16)	0.42267 (15)	0.48335 (13)	0.0428 (4)	
C9	0.3295 (3)	0.3851 (3)	0.1726 (2)	0.0555 (7)	
H9A	0.3059	0.3566	0.0960	0.083*	
H9B	0.3427	0.3203	0.2057	0.083*	
H9C	0.4179	0.4649	0.2110	0.083*	
C10	0.0209 (3)	0.3430 (3)	−0.02031 (19)	0.0549 (7)	
H10A	0.0864	0.3248	−0.0419	0.082*	
H10B	0.0020	0.4090	−0.0486	0.082*	
H10C	−0.0691	0.2656	−0.0500	0.082*	
O11	0.42842 (15)	0.54477 (15)	0.57733 (12)	0.0394 (4)	
C12	0.2703 (2)	0.6577 (2)	0.49445 (16)	0.0313 (5)	
C13	0.3465 (2)	0.7583 (2)	0.46804 (17)	0.0340 (5)	
C14	0.3132 (2)	0.8603 (2)	0.4713 (2)	0.0456 (6)	
H14	0.3587	0.9279	0.4496	0.055*	
C15	0.2158 (3)	0.8659 (3)	0.5053 (2)	0.0511 (7)	
H15	0.1967	0.9376	0.5080	0.061*	
C16	0.1460 (2)	0.7684 (2)	0.5353 (2)	0.0444 (6)	
H16	0.0812	0.7738	0.5609	0.053*	
C17	0.1709 (2)	0.6631 (2)	0.52787 (18)	0.0373 (5)	
H17	0.1203	0.5939	0.5456	0.045*	
C18	0.4645 (2)	0.7643 (2)	0.44320 (17)	0.0321 (5)	
C19	0.4541 (2)	0.7587 (2)	0.34031 (18)	0.0359 (5)	
H19	0.3693	0.7501	0.2824	0.043*	0.196 (5)
C20	0.5692 (2)	0.7658 (2)	0.32386 (18)	0.0370 (5)	
H20	0.5606	0.7589	0.2532	0.044*	
C21	0.6961 (2)	0.7827 (2)	0.40713 (18)	0.0338 (5)	
C22	0.7064 (2)	0.7918 (2)	0.50938 (17)	0.0337 (5)	
H22	0.7930	0.8045	0.5680	0.040*	
C23	0.5928 (2)	0.7827 (2)	0.52734 (18)	0.0348 (5)	
H23	0.6020	0.7891	0.5981	0.042*	0.804 (5)
C24	0.3237 (6)	0.7510 (7)	0.2442 (8)	0.0442 (9)	0.597 (3)

H24A	0.3168	0.7070	0.1756	0.053*	0.597 (3)
H24B	0.2364	0.6991	0.2479	0.053*	0.597 (3)
O25	0.3283 (3)	0.8716 (3)	0.2413 (3)	0.0473 (9)	0.597 (3)
C26	0.4243 (6)	0.9416 (6)	0.2061 (5)	0.0531 (13)	0.597 (3)
H26A	0.3970	0.8932	0.1316	0.064*	0.597 (3)
H26B	0.5226	0.9568	0.2550	0.064*	0.597 (3)
C27	0.418 (2)	1.0650 (11)	0.2077 (15)	0.074 (4)	0.597 (3)
H27A	0.3218	1.0491	0.1560	0.111*	0.597 (3)
H27B	0.4874	1.1164	0.1871	0.111*	0.597 (3)
H27C	0.4411	1.1105	0.2809	0.111*	0.597 (3)
C24A	0.3197 (13)	0.7516 (18)	0.247 (2)	0.0442 (9)	0.223 (3)
H24C	0.2649	0.6655	0.1929	0.053*	0.223 (3)
H24D	0.2580	0.7659	0.2768	0.053*	0.223 (3)
O25A	0.3552 (10)	0.8435 (8)	0.1949 (6)	0.048 (2)	0.223 (3)
C26A	0.4003 (17)	0.9690 (11)	0.2589 (11)	0.058 (3)	0.223 (3)
H26C	0.4812	0.9911	0.3312	0.069*	0.223 (3)
H26D	0.3210	0.9747	0.2695	0.069*	0.223 (3)
C27A	0.445 (7)	1.059 (3)	0.202 (4)	0.10 (2)	0.223 (3)
H27D	0.5305	1.0597	0.1989	0.156*	0.223 (3)
H27E	0.4672	1.1444	0.2416	0.156*	0.223 (3)
H27F	0.3678	1.0316	0.1279	0.156*	0.223 (3)
C24B	0.6216 (14)	0.8239 (10)	0.6481 (7)	0.046 (3)	0.180 (2)
H24E	0.5381	0.7668	0.6537	0.055*	0.180 (2)
H24F	0.7054	0.8133	0.6952	0.055*	0.180 (2)
O25B	0.6473 (10)	0.9521 (9)	0.6873 (7)	0.062 (3)	0.180 (2)
C26B	0.661 (2)	0.989 (2)	0.7931 (11)	0.084 (7)	0.180 (2)
H26E	0.7206	1.0815	0.8283	0.101*	0.180 (2)
H26F	0.7085	0.9455	0.8383	0.101*	0.180 (2)
C27B	0.517 (3)	0.953 (5)	0.785 (3)	0.102 (15)	0.180 (2)
H27G	0.4667	0.9887	0.7338	0.153*	0.180 (2)
H27H	0.5268	0.9867	0.8564	0.153*	0.180 (2)
H27I	0.4626	0.8603	0.7583	0.153*	0.180 (2)
C28	0.8235 (2)	0.7896 (2)	0.39342 (19)	0.0409 (6)	
H28A	0.9107	0.8600	0.4552	0.049*	
H28B	0.8314	0.7097	0.3971	0.049*	
N29	0.81986 (19)	0.80880 (18)	0.29298 (15)	0.0366 (5)	
C30	0.8737 (2)	0.9260 (2)	0.28282 (19)	0.0366 (5)	
C31	0.8470 (3)	0.9017 (2)	0.1664 (2)	0.0488 (6)	
N32	0.7736 (3)	0.7646 (2)	0.11856 (17)	0.0565 (6)	
C33	0.7617 (3)	0.7183 (2)	0.1919 (2)	0.0464 (6)	
C34	0.7501 (9)	0.9575 (11)	0.1012 (14)	0.076 (4)	0.571 (18)
H34A	0.7020	0.9125	0.0221	0.091*	0.571 (18)
H34B	0.6769	0.9531	0.1244	0.091*	0.571 (18)
C35	0.8569 (12)	1.0950 (8)	0.1302 (9)	0.087 (3)	0.571 (18)
H35A	0.8194	1.1330	0.0744	0.104*	0.571 (18)
H35B	0.8795	1.1473	0.2018	0.104*	0.571 (18)
C36	0.9880 (14)	1.0840 (10)	0.1331 (15)	0.120 (5)	0.571 (18)
H36A	0.9911	1.0881	0.0642	0.144*	0.571 (18)

H36B	1.0761	1.1547	0.1938	0.144*	0.571 (18)
C37	0.9781 (9)	0.9583 (10)	0.1483 (12)	0.056 (3)	0.571 (18)
H37A	1.0656	0.9710	0.2119	0.068*	0.571 (18)
H37B	0.9657	0.9014	0.0829	0.068*	0.571 (18)
C34A	0.7726 (14)	0.9806 (15)	0.1167 (18)	0.063 (3)	0.429 (18)
H34C	0.6816	0.9248	0.0499	0.075*	0.429 (18)
H34D	0.7513	1.0235	0.1690	0.075*	0.429 (18)
C35A	0.8720 (15)	1.0774 (15)	0.0901 (16)	0.103 (5)	0.429 (18)
H35C	0.8655	1.1586	0.1030	0.124*	0.429 (18)
H35D	0.8507	1.0461	0.0136	0.124*	0.429 (18)
C36A	1.0181 (13)	1.0931 (10)	0.1682 (10)	0.063 (3)	0.429 (18)
H36C	1.0863	1.1237	0.1393	0.076*	0.429 (18)
H36D	1.0556	1.1551	0.2399	0.076*	0.429 (18)
C37A	0.9983 (11)	0.9658 (15)	0.1786 (16)	0.063 (4)	0.429 (18)
H37C	1.0705	0.9738	0.2504	0.075*	0.429 (18)
H37D	1.0067	0.9160	0.1210	0.075*	0.429 (18)
O38	0.93176 (19)	1.02622 (17)	0.35434 (14)	0.0521 (5)	
C39	0.6958 (7)	0.5796 (3)	0.1755 (6)	0.0643 (9)	0.804 (5)
H39A	0.6393	0.5635	0.2153	0.077*	0.804 (5)
H39B	0.6287	0.5341	0.0972	0.077*	0.804 (5)
C40	0.7963 (3)	0.5268 (3)	0.2108 (3)	0.0489 (10)	0.804 (5)
H40A	0.8622	0.5708	0.2894	0.059*	0.804 (5)
H40B	0.8540	0.5440	0.1720	0.059*	0.804 (5)
C41	0.7258 (5)	0.3833 (4)	0.1911 (4)	0.0616 (11)	0.804 (5)
H41A	0.8010	0.3570	0.2269	0.074*	0.804 (5)
H41B	0.6623	0.3650	0.2251	0.074*	0.804 (5)
C42	0.6397 (7)	0.3055 (6)	0.0718 (5)	0.089 (2)	0.804 (5)
H42A	0.5606	0.3264	0.0368	0.134*	0.804 (5)
H42B	0.6015	0.2149	0.0642	0.134*	0.804 (5)
H42C	0.7012	0.3248	0.0370	0.134*	0.804 (5)
C39A	0.686 (3)	0.5810 (8)	0.178 (2)	0.0643 (9)	0.196 (5)
H39C	0.7189	0.5718	0.2512	0.077*	0.196 (5)
H39D	0.5832	0.5577	0.1480	0.077*	0.196 (5)
C40A	0.7002 (16)	0.4884 (10)	0.1112 (13)	0.061 (4)	0.196 (5)
H40C	0.8020	0.5227	0.1283	0.073*	0.196 (5)
H40D	0.6453	0.4816	0.0345	0.073*	0.196 (5)
C41A	0.653 (3)	0.3537 (13)	0.1184 (17)	0.060 (5)	0.196 (5)
H41C	0.7321	0.3514	0.1803	0.072*	0.196 (5)
H41D	0.5701	0.3305	0.1322	0.072*	0.196 (5)
C42A	0.614 (3)	0.2575 (18)	0.0147 (19)	0.110 (9)	0.196 (5)
H42D	0.6794	0.2949	−0.0141	0.164*	0.196 (5)
H42E	0.5158	0.2336	−0.0391	0.164*	0.196 (5)
H42F	0.6215	0.1818	0.0305	0.164*	0.196 (5)

Atomic displacement parameters (Å²)

	U^{11}	U^{22}	U^{33}	U^{12}	U^{13}	U^{23}
O1	0.0417 (9)	0.0646 (12)	0.0406 (10)	0.0347 (9)	0.0127 (8)	0.0158 (8)

N2	0.0399 (11)	0.0612 (14)	0.0350 (11)	0.0315 (11)	0.0121 (9)	0.0115 (10)
C3	0.0317 (11)	0.0316 (12)	0.0369 (13)	0.0185 (10)	0.0147 (10)	0.0115 (10)
C4	0.0365 (12)	0.0328 (13)	0.0393 (13)	0.0185 (10)	0.0182 (10)	0.0127 (10)
C5	0.0438 (13)	0.0387 (14)	0.0418 (13)	0.0248 (11)	0.0201 (12)	0.0145 (11)
N6	0.0298 (10)	0.0410 (11)	0.0337 (10)	0.0218 (9)	0.0135 (9)	0.0118 (8)
S7	0.0339 (3)	0.0411 (4)	0.0370 (3)	0.0254 (3)	0.0197 (3)	0.0183 (3)
O8	0.0435 (9)	0.0437 (10)	0.0609 (11)	0.0258 (8)	0.0332 (8)	0.0287 (8)
C9	0.0464 (15)	0.080 (2)	0.0410 (15)	0.0344 (15)	0.0199 (12)	0.0080 (13)
C10	0.0645 (17)	0.0577 (18)	0.0396 (14)	0.0355 (15)	0.0147 (13)	0.0140 (12)
O11	0.0404 (9)	0.0557 (11)	0.0350 (8)	0.0339 (8)	0.0172 (7)	0.0191 (7)
C12	0.0292 (11)	0.0372 (13)	0.0325 (12)	0.0211 (10)	0.0133 (9)	0.0121 (10)
C13	0.0284 (11)	0.0383 (13)	0.0394 (13)	0.0200 (10)	0.0158 (10)	0.0113 (10)
C14	0.0400 (13)	0.0387 (15)	0.0682 (17)	0.0228 (12)	0.0290 (13)	0.0209 (13)
C15	0.0457 (14)	0.0442 (16)	0.0774 (19)	0.0306 (13)	0.0332 (14)	0.0176 (14)
C16	0.0381 (13)	0.0493 (16)	0.0596 (16)	0.0292 (12)	0.0280 (12)	0.0151 (12)
C17	0.0337 (12)	0.0452 (15)	0.0427 (13)	0.0234 (11)	0.0211 (10)	0.0156 (11)
C18	0.0316 (11)	0.0306 (12)	0.0424 (13)	0.0185 (10)	0.0201 (10)	0.0139 (10)
C19	0.0324 (12)	0.0384 (13)	0.0409 (13)	0.0189 (10)	0.0176 (10)	0.0147 (10)
C20	0.0409 (13)	0.0451 (14)	0.0372 (13)	0.0257 (11)	0.0220 (11)	0.0185 (11)
C21	0.0365 (12)	0.0350 (13)	0.0441 (13)	0.0214 (10)	0.0249 (11)	0.0202 (10)
C22	0.0288 (11)	0.0425 (14)	0.0371 (12)	0.0203 (10)	0.0163 (10)	0.0191 (10)
C23	0.0329 (12)	0.0410 (14)	0.0379 (12)	0.0207 (10)	0.0189 (10)	0.0153 (10)
C24	0.0360 (16)	0.054 (2)	0.0436 (18)	0.0238 (14)	0.0144 (14)	0.0201 (15)
O25	0.0471 (19)	0.062 (3)	0.053 (2)	0.0366 (18)	0.0268 (17)	0.0335 (19)
C26	0.060 (3)	0.049 (4)	0.057 (3)	0.027 (3)	0.028 (3)	0.025 (3)
C27	0.112 (10)	0.072 (6)	0.074 (7)	0.056 (7)	0.057 (7)	0.042 (5)
C24A	0.0360 (16)	0.054 (2)	0.0436 (18)	0.0238 (14)	0.0144 (14)	0.0201 (15)
O25A	0.050 (5)	0.062 (6)	0.042 (5)	0.029 (5)	0.023 (4)	0.029 (4)
C26A	0.052 (8)	0.054 (7)	0.070 (9)	0.028 (7)	0.027 (7)	0.019 (6)
C27A	0.10 (3)	0.071 (15)	0.08 (2)	0.00 (2)	0.018 (18)	0.038 (17)
C24B	0.040 (7)	0.057 (8)	0.055 (8)	0.030 (7)	0.028 (6)	0.021 (6)
O25B	0.052 (6)	0.063 (6)	0.061 (6)	0.022 (5)	0.028 (5)	−0.003 (5)
C26B	0.081 (13)	0.100 (18)	0.056 (10)	0.045 (13)	0.026 (11)	−0.009 (11)
C27B	0.102 (18)	0.13 (3)	0.058 (18)	0.05 (2)	0.046 (16)	−0.015 (17)
C28	0.0438 (13)	0.0577 (16)	0.0488 (14)	0.0345 (12)	0.0319 (12)	0.0314 (12)
N29	0.0428 (11)	0.0412 (12)	0.0424 (11)	0.0239 (9)	0.0287 (9)	0.0198 (9)
C30	0.0374 (12)	0.0419 (15)	0.0456 (14)	0.0253 (11)	0.0251 (11)	0.0185 (12)
C31	0.0663 (17)	0.0475 (16)	0.0544 (16)	0.0304 (14)	0.0410 (14)	0.0260 (13)
N32	0.0764 (16)	0.0533 (15)	0.0528 (13)	0.0270 (12)	0.0441 (12)	0.0176 (11)
C33	0.0554 (15)	0.0426 (15)	0.0570 (16)	0.0243 (13)	0.0385 (13)	0.0173 (12)
C34	0.088 (5)	0.078 (6)	0.061 (6)	0.046 (5)	0.022 (5)	0.037 (5)
C35	0.141 (7)	0.072 (5)	0.088 (6)	0.068 (5)	0.064 (5)	0.052 (4)
C36	0.122 (8)	0.097 (7)	0.154 (11)	0.037 (6)	0.071 (8)	0.086 (7)
C37	0.087 (4)	0.053 (4)	0.067 (7)	0.033 (4)	0.067 (5)	0.032 (4)
C34A	0.088 (6)	0.060 (7)	0.051 (7)	0.038 (6)	0.034 (6)	0.028 (5)
C35A	0.098 (7)	0.085 (8)	0.109 (9)	0.019 (6)	0.041 (7)	0.062 (7)
C36A	0.098 (6)	0.052 (5)	0.049 (5)	0.028 (4)	0.046 (4)	0.023 (3)
C37A	0.093 (5)	0.060 (6)	0.052 (7)	0.027 (4)	0.056 (5)	0.022 (4)

O38	0.0614 (11)	0.0445 (11)	0.0570 (11)	0.0263 (9)	0.0320 (9)	0.0144 (9)
C39	0.073 (2)	0.0480 (18)	0.086 (2)	0.0241 (16)	0.0522 (18)	0.0228 (15)
C40	0.0466 (19)	0.047 (2)	0.055 (2)	0.0208 (16)	0.0263 (17)	0.0176 (16)
C41	0.069 (3)	0.056 (2)	0.083 (3)	0.037 (2)	0.047 (2)	0.033 (2)
C42	0.083 (4)	0.060 (4)	0.103 (5)	0.028 (4)	0.036 (4)	−0.003 (3)
C39A	0.073 (2)	0.0480 (18)	0.086 (2)	0.0241 (16)	0.0522 (18)	0.0228 (15)
C40A	0.059 (8)	0.042 (7)	0.085 (10)	0.027 (6)	0.037 (7)	0.011 (6)
C41A	0.073 (11)	0.058 (8)	0.057 (11)	0.036 (10)	0.029 (10)	0.027 (8)
C42A	0.093 (15)	0.072 (12)	0.127 (19)	0.032 (13)	0.044 (16)	−0.029 (12)

Geometric parameters (Å, º)

O1—C5	1.349 (3)	C26B—C27B	1.486 (15)
O1—N2	1.419 (2)	C26B—H26E	0.9900
N2—C3	1.302 (3)	C26B—H26F	0.9900
C3—N6	1.390 (3)	C27B—H27G	0.9800
C3—C4	1.418 (3)	C27B—H27H	0.9800
C4—C5	1.350 (3)	C27B—H27I	0.9800
C4—C9	1.481 (3)	C28—N29	1.451 (3)
C5—C10	1.484 (3)	C28—H28A	0.9900
N6—S7	1.626 (2)	C28—H28B	0.9900
N6—H6	0.875 (10)	N29—C30	1.362 (3)
S7—O8	1.4221 (16)	N29—C33	1.399 (3)
S7—O11	1.4334 (15)	C30—O38	1.209 (3)
S7—C12	1.766 (2)	C30—C31	1.510 (3)
C9—H9A	0.9800	C31—N32	1.448 (3)
C9—H9B	0.9800	C31—C37	1.537 (6)
C9—H9C	0.9800	C31—C37A	1.538 (7)
C10—H10A	0.9800	C31—C34A	1.540 (7)
C10—H10B	0.9800	C31—C34	1.549 (6)
C10—H10C	0.9800	N32—C33	1.266 (3)
C12—C17	1.395 (3)	C33—C39	1.489 (4)
C12—C13	1.399 (3)	C33—C39A	1.492 (8)
C13—C14	1.391 (3)	C34—C35	1.528 (7)
C13—C18	1.489 (3)	C34—H34A	0.9900
C14—C15	1.379 (3)	C34—H34B	0.9900
C14—H14	0.9500	C35—C36	1.522 (7)
C15—C16	1.376 (3)	C35—H35A	0.9900
C15—H15	0.9500	C35—H35B	0.9900
C16—C17	1.376 (3)	C36—C37	1.510 (6)
C16—H16	0.9500	C36—H36A	0.9900
C17—H17	0.9500	C36—H36B	0.9900
C18—C23	1.392 (3)	C37—H37A	0.9900
C18—C19	1.397 (3)	C37—H37B	0.9900
C19—C20	1.387 (3)	C34A—C35A	1.504 (12)
C19—C24	1.534 (4)	C34A—H34C	0.9900
C19—C24A	1.544 (8)	C34A—H34D	0.9900
C19—H19	0.9500	C35A—C36A	1.518 (12)

C20—C21	1.383 (3)	C35A—H35C	0.9900
C20—H20	0.9500	C35A—H35D	0.9900
C21—C22	1.384 (3)	C36A—C37A	1.486 (11)
C21—C28	1.505 (3)	C36A—H36C	0.9900
C22—C23	1.376 (3)	C36A—H36D	0.9900
C22—H22	0.9500	C37A—H37C	0.9900
C23—C24B	1.568 (8)	C37A—H37D	0.9900
C23—H23	0.9500	C39—C40	1.447 (7)
C24—O25	1.422 (7)	C39—H39A	0.9900
C24—H24A	0.9900	C39—H39B	0.9900
C24—H24B	0.9900	C40—C41	1.535 (4)
O25—C26	1.418 (5)	C40—H40A	0.9900
C26—C27	1.489 (13)	C40—H40B	0.9900
C26—H26A	0.9900	C41—C42	1.512 (6)
C26—H26B	0.9900	C41—H41A	0.9900
C27—H27A	0.9800	C41—H41B	0.9900
C27—H27B	0.9800	C42—H42A	0.9800
C27—H27C	0.9800	C42—H42B	0.9800
C24A—O25A	1.428 (9)	C42—H42C	0.9800
C24A—H24C	0.9900	C39A—C40A	1.435 (10)
C24A—H24D	0.9900	C39A—H39C	0.9900
O25A—C26A	1.422 (8)	C39A—H39D	0.9900
C26A—C27A	1.487 (16)	C40A—C41A	1.529 (10)
C26A—H26C	0.9900	C40A—H40C	0.9900
C26A—H26D	0.9900	C40A—H40D	0.9900
C27A—H27D	0.9800	C41A—C42A	1.516 (11)
C27A—H27E	0.9800	C41A—H41C	0.9900
C27A—H27F	0.9800	C41A—H41D	0.9900
C24B—O25B	1.427 (8)	C42A—H42D	0.9800
C24B—H24E	0.9900	C42A—H42E	0.9800
C24B—H24F	0.9900	C42A—H42F	0.9800
O25B—C26B	1.422 (9)		

C5—O1—N2	109.03 (16)	C26B—C27B—H27I	109.5
C3—N2—O1	103.49 (18)	H27G—C27B—H27I	109.5
N2—C3—N6	120.7 (2)	H27H—C27B—H27I	109.5
N2—C3—C4	114.27 (19)	N29—C28—C21	115.00 (17)
N6—C3—C4	125.0 (2)	N29—C28—H28A	108.5
C5—C4—C3	102.7 (2)	C21—C28—H28A	108.5
C5—C4—C9	129.1 (2)	N29—C28—H28B	108.5
C3—C4—C9	128.1 (2)	C21—C28—H28B	108.5
O1—C5—C4	110.5 (2)	H28A—C28—H28B	107.5
O1—C5—C10	116.2 (2)	C30—N29—C33	107.80 (18)
C4—C5—C10	133.3 (2)	C30—N29—C28	123.1 (2)
C3—N6—S7	125.38 (16)	C33—N29—C28	129.1 (2)
C3—N6—H6	119.6 (17)	O38—C30—N29	125.7 (2)
S7—N6—H6	113.7 (17)	O38—C30—C31	129.0 (2)
O8—S7—O11	118.46 (9)	N29—C30—C31	105.3 (2)

O8—S7—N6	109.65 (10)	N32—C31—C30	104.82 (18)
O11—S7—N6	103.87 (9)	N32—C31—C37	111.0 (5)
O8—S7—C12	107.07 (10)	C30—C31—C37	117.0 (6)
O11—S7—C12	109.99 (10)	N32—C31—C37A	115.5 (7)
N6—S7—C12	107.35 (10)	C30—C31—C37A	103.0 (8)
C4—C9—H9A	109.5	N32—C31—C34A	118.9 (8)
C4—C9—H9B	109.5	C30—C31—C34A	108.1 (9)
H9A—C9—H9B	109.5	C37A—C31—C34A	105.2 (7)
C4—C9—H9C	109.5	N32—C31—C34	108.5 (5)
H9A—C9—H9C	109.5	C30—C31—C34	113.1 (7)
H9B—C9—H9C	109.5	C37—C31—C34	102.4 (5)
C5—C10—H10A	109.5	C33—N32—C31	107.6 (2)
C5—C10—H10B	109.5	N32—C33—N29	114.5 (2)
H10A—C10—H10B	109.5	N32—C33—C39	123.9 (3)
C5—C10—H10C	109.5	N29—C33—C39	121.6 (3)
H10A—C10—H10C	109.5	N32—C33—C39A	126.3 (10)
H10B—C10—H10C	109.5	N29—C33—C39A	119.2 (9)
C17—C12—C13	121.1 (2)	C35—C34—C31	102.3 (5)
C17—C12—S7	115.07 (17)	C35—C34—H34A	111.3
C13—C12—S7	123.78 (17)	C31—C34—H34A	111.3
C14—C13—C12	116.9 (2)	C35—C34—H34B	111.3
C14—C13—C18	119.4 (2)	C31—C34—H34B	111.3
C12—C13—C18	123.65 (19)	H34A—C34—H34B	109.2
C15—C14—C13	121.7 (2)	C36—C35—C34	103.6 (6)
C15—C14—H14	119.1	C36—C35—H35A	111.0
C13—C14—H14	119.1	C34—C35—H35A	111.0
C16—C15—C14	120.6 (2)	C36—C35—H35B	111.0
C16—C15—H15	119.7	C34—C35—H35B	111.0
C14—C15—H15	119.7	H35A—C35—H35B	109.0
C15—C16—C17	119.3 (2)	C37—C36—C35	107.9 (5)
C15—C16—H16	120.4	C37—C36—H36A	110.1
C17—C16—H16	120.4	C35—C36—H36A	110.1
C16—C17—C12	120.2 (2)	C37—C36—H36B	110.1
C16—C17—H17	119.9	C35—C36—H36B	110.1
C12—C17—H17	119.9	H36A—C36—H36B	108.4
C23—C18—C19	118.8 (2)	C36—C37—C31	105.6 (5)
C23—C18—C13	118.55 (19)	C36—C37—H37A	110.6
C19—C18—C13	122.58 (18)	C31—C37—H37A	110.6
C20—C19—C18	119.12 (19)	C36—C37—H37B	110.6
C20—C19—C24	117.3 (5)	C31—C37—H37B	110.6
C18—C19—C24	123.5 (5)	H37A—C37—H37B	108.8
C20—C19—C24A	120.0 (12)	C35A—C34A—C31	107.8 (8)
C18—C19—C24A	120.8 (12)	C35A—C34A—H34C	110.2
C20—C19—H19	120.4	C31—C34A—H34C	110.2
C18—C19—H19	120.4	C35A—C34A—H34D	110.2
C21—C20—C19	122.1 (2)	C31—C34A—H34D	110.2
C21—C20—H20	119.0	H34C—C34A—H34D	108.5
C19—C20—H20	119.0	C34A—C35A—C36A	103.0 (9)

C20—C21—C22	118.2 (2)	C34A—C35A—H35C	111.2
C20—C21—C28	124.2 (2)	C36A—C35A—H35C	111.2
C22—C21—C28	117.64 (18)	C34A—C35A—H35D	111.2
C23—C22—C21	120.88 (19)	C36A—C35A—H35D	111.2
C23—C22—H22	119.6	H35C—C35A—H35D	109.1
C21—C22—H22	119.6	C37A—C36A—C35A	106.5 (8)
C22—C23—C18	120.9 (2)	C37A—C36A—H36C	110.4
C22—C23—C24B	118.0 (5)	C35A—C36A—H36C	110.4
C18—C23—C24B	119.7 (5)	C37A—C36A—H36D	110.4
C22—C23—H23	119.5	C35A—C36A—H36D	110.4
C18—C23—H23	119.5	H36C—C36A—H36D	108.6
O25—C24—C19	113.6 (5)	C36A—C37A—C31	105.1 (8)
O25—C24—H24A	108.8	C36A—C37A—H37C	110.7
C19—C24—H24A	108.8	C31—C37A—H37C	110.7
O25—C24—H24B	108.8	C36A—C37A—H37D	110.7
C19—C24—H24B	108.8	C31—C37A—H37D	110.7
H24A—C24—H24B	107.7	H37C—C37A—H37D	108.8
C26—O25—C24	114.4 (6)	C40—C39—C33	114.8 (4)
O25—C26—C27	108.4 (9)	C40—C39—H39A	108.6
O25—C26—H26A	110.0	C33—C39—H39A	108.6
C27—C26—H26A	110.0	C40—C39—H39B	108.6
O25—C26—H26B	110.0	C33—C39—H39B	108.6
C27—C26—H26B	110.0	H39A—C39—H39B	107.5
H26A—C26—H26B	108.4	C39—C40—C41	113.9 (3)
C26—C27—H27A	109.5	C39—C40—H40A	108.8
C26—C27—H27B	109.5	C41—C40—H40A	108.8
H27A—C27—H27B	109.5	C39—C40—H40B	108.8
C26—C27—H27C	109.5	C41—C40—H40B	108.8
H27A—C27—H27C	109.5	H40A—C40—H40B	107.7
H27B—C27—H27C	109.5	C42—C41—C40	113.1 (4)
O25A—C24A—C19	112.0 (8)	C42—C41—H41A	109.0
O25A—C24A—H24C	109.2	C40—C41—H41A	109.0
C19—C24A—H24C	109.2	C42—C41—H41B	109.0
O25A—C24A—H24D	109.2	C40—C41—H41B	109.0
C19—C24A—H24D	109.2	H41A—C41—H41B	107.8
H24C—C24A—H24D	107.9	C41—C42—H42A	109.5
C26A—O25A—C24A	112.7 (13)	C41—C42—H42B	109.5
O25A—C26A—C27A	108.8 (16)	H42A—C42—H42B	109.5
O25A—C26A—H26C	109.9	C41—C42—H42C	109.5
C27A—C26A—H26C	109.9	H42A—C42—H42C	109.5
O25A—C26A—H26D	109.9	H42B—C42—H42C	109.5
C27A—C26A—H26D	109.9	C40A—C39A—C33	119.7 (10)
H26C—C26A—H26D	108.3	C40A—C39A—H39C	107.4
C26A—C27A—H27D	109.5	C33—C39A—H39C	107.4
C26A—C27A—H27E	109.5	C40A—C39A—H39D	107.4
H27D—C27A—H27E	109.5	C33—C39A—H39D	107.4
C26A—C27A—H27F	109.5	H39C—C39A—H39D	106.9
H27D—C27A—H27F	109.5	C39A—C40A—C41A	119.2 (11)

H27E—C27A—H27F	109.5	C39A—C40A—H40C	107.5
O25B—C24B—C23	113.4 (8)	C41A—C40A—H40C	107.5
O25B—C24B—H24E	108.9	C39A—C40A—H40D	107.5
C23—C24B—H24E	108.9	C41A—C40A—H40D	107.5
O25B—C24B—H24F	108.9	H40C—C40A—H40D	107.0
C23—C24B—H24F	108.9	C42A—C41A—C40A	111.7 (13)
H24E—C24B—H24F	107.7	C42A—C41A—H41C	109.3
C26B—O25B—C24B	114.6 (12)	C40A—C41A—H41C	109.3
O25B—C26B—C27B	109.3 (15)	C42A—C41A—H41D	109.3
O25B—C26B—H26E	109.8	C40A—C41A—H41D	109.3
C27B—C26B—H26E	109.8	H41C—C41A—H41D	107.9
O25B—C26B—H26F	109.8	C41A—C42A—H42D	109.5
C27B—C26B—H26F	109.8	C41A—C42A—H42E	109.5
H26E—C26B—H26F	108.3	H42D—C42A—H42E	109.5
C26B—C27B—H27G	109.5	C41A—C42A—H42F	109.5
C26B—C27B—H27H	109.5	H42D—C42A—H42F	109.5
H27G—C27B—H27H	109.5	H42E—C42A—H42F	109.5

C5—O1—N2—C3	−0.4 (2)	C18—C19—C24A—O25A	130.2 (17)
O1—N2—C3—N6	−179.66 (18)	C19—C24A—O25A—C26A	−74 (2)
O1—N2—C3—C4	0.9 (2)	C24A—O25A—C26A—C27A	176 (3)
N2—C3—C4—C5	−1.0 (3)	C22—C23—C24B—O25B	95.0 (9)
N6—C3—C4—C5	179.5 (2)	C18—C23—C24B—O25B	−71.6 (10)
N2—C3—C4—C9	−179.7 (2)	C23—C24B—O25B—C26B	174.6 (11)
N6—C3—C4—C9	0.9 (4)	C24B—O25B—C26B—C27B	−86 (3)
N2—O1—C5—C4	−0.2 (3)	C20—C21—C28—N29	14.6 (3)
N2—O1—C5—C10	178.92 (19)	C22—C21—C28—N29	−166.5 (2)
C3—C4—C5—O1	0.7 (2)	C21—C28—N29—C30	89.5 (3)
C9—C4—C5—O1	179.3 (2)	C21—C28—N29—C33	−88.9 (3)
C3—C4—C5—C10	−178.2 (3)	C33—N29—C30—O38	179.8 (2)
C9—C4—C5—C10	0.4 (4)	C28—N29—C30—O38	1.1 (3)
N2—C3—N6—S7	3.2 (3)	C33—N29—C30—C31	−1.1 (2)
C4—C3—N6—S7	−177.40 (17)	C28—N29—C30—C31	−179.75 (19)
C3—N6—S7—O8	55.5 (2)	O38—C30—C31—N32	−179.8 (2)
C3—N6—S7—O11	−176.99 (18)	N29—C30—C31—N32	1.1 (2)
C3—N6—S7—C12	−60.5 (2)	N29—C30—C31—C37	−122.2 (4)
O8—S7—C12—C17	21.51 (19)	O38—C30—C31—C37A	59.0 (7)
O11—S7—C12—C17	−108.44 (17)	N29—C30—C31—C37A	−120.1 (6)
N6—S7—C12—C17	139.18 (16)	O38—C30—C31—C34A	−52.0 (6)
O8—S7—C12—C13	−159.41 (17)	N29—C30—C31—C34A	128.9 (6)
O11—S7—C12—C13	70.64 (19)	N29—C30—C31—C34	119.2 (4)
N6—S7—C12—C13	−41.7 (2)	C30—C31—N32—C33	−0.7 (3)
C17—C12—C13—C14	−3.2 (3)	C37—C31—N32—C33	126.4 (6)
S7—C12—C13—C14	177.76 (17)	C37A—C31—N32—C33	111.8 (8)
C17—C12—C13—C18	173.3 (2)	C34A—C31—N32—C33	−121.6 (8)
S7—C12—C13—C18	−5.7 (3)	C34—C31—N32—C33	−121.9 (7)
C12—C13—C14—C15	3.8 (3)	C31—N32—C33—N29	0.1 (3)
C18—C13—C14—C15	−172.9 (2)	C31—N32—C33—C39	−178.1 (4)

C13—C14—C15—C16	−1.2 (4)	C31—N32—C33—C39A	176.5 (13)
C14—C15—C16—C17	−2.0 (4)	C30—N29—C33—N32	0.6 (3)
C15—C16—C17—C12	2.6 (4)	C28—N29—C33—N32	179.2 (2)
C13—C12—C17—C16	0.1 (3)	C30—N29—C33—C39	178.9 (3)
S7—C12—C17—C16	179.19 (18)	C28—N29—C33—C39	−2.5 (5)
C14—C13—C18—C23	106.7 (2)	C30—N29—C33—C39A	−176.0 (13)
C12—C13—C18—C23	−69.7 (3)	C28—N29—C33—C39A	2.6 (13)
C14—C13—C18—C19	−69.9 (3)	N32—C31—C34—C35	−159.5 (8)
C12—C13—C18—C19	113.7 (2)	C30—C31—C34—C35	84.6 (10)
C23—C18—C19—C20	2.9 (3)	C37—C31—C34—C35	−42.1 (13)
C13—C18—C19—C20	179.5 (2)	C31—C34—C35—C36	38.6 (16)
C23—C18—C19—C24	−174.2 (3)	C34—C35—C36—C37	−20.6 (16)
C13—C18—C19—C24	2.4 (4)	C35—C36—C37—C31	−5.8 (14)
C23—C18—C19—C24A	−173.9 (8)	N32—C31—C37—C36	145.1 (8)
C13—C18—C19—C24A	2.7 (9)	C30—C31—C37—C36	−94.7 (8)
C18—C19—C20—C21	−2.2 (3)	C34—C31—C37—C36	29.5 (11)
C24—C19—C20—C21	175.1 (4)	N32—C31—C34A—C35A	−125.5 (15)
C24A—C19—C20—C21	174.6 (9)	C30—C31—C34A—C35A	115.3 (16)
C19—C20—C21—C22	0.3 (3)	C37A—C31—C34A—C35A	6 (2)
C19—C20—C21—C28	179.3 (2)	C31—C34A—C35A—C36A	−25 (2)
C20—C21—C22—C23	0.8 (3)	C34A—C35A—C36A—C37A	36 (2)
C28—C21—C22—C23	−178.2 (2)	C35A—C36A—C37A—C31	−32.4 (14)
C21—C22—C23—C18	−0.1 (3)	N32—C31—C37A—C36A	149.4 (8)
C21—C22—C23—C24B	−166.5 (5)	C30—C31—C37A—C36A	−97.0 (10)
C19—C18—C23—C22	−1.8 (3)	C34A—C31—C37A—C36A	16.1 (16)
C13—C18—C23—C22	−178.5 (2)	N32—C33—C39—C40	97.0 (5)
C19—C18—C23—C24B	164.4 (5)	N29—C33—C39—C40	−81.1 (5)
C13—C18—C23—C24B	−12.3 (6)	C33—C39—C40—C41	−178.9 (4)
C20—C19—C24—O25	−91.0 (9)	C39—C40—C41—C42	67.0 (5)
C18—C19—C24—O25	86.1 (7)	N32—C33—C39A—C40A	41 (3)
C19—C24—O25—C26	75.1 (10)	N29—C33—C39A—C40A	−143.0 (19)
C24—O25—C26—C27	−179.8 (9)	C33—C39A—C40A—C41A	166 (2)
C20—C19—C24A—O25A	−47 (2)	C39A—C40A—C41A—C42A	155 (2)

Hydrogen-bond geometry (Å, º)

D—H···*A*	*D*—H	H···*A*	*D*···*A*	*D*—H···*A*
N6—H6···O11^{i}	0.88 (1)	2.12 (1)	2.951 (2)	159 (2)
C28—H28*A*···O38^{ii}	0.99	2.40	3.318 (3)	153
C28—H28*B*···O8^{i}	0.99	2.46	3.265 (3)	138

Symmetry codes: (i) −*x*+1, −*y*+1, −*z*+1; (ii) −*x*+2, −*y*+2, −*z*+1.